Journal of Applied Polymer Science

Chitosan/MWCNTs-Decorated with Silver Nanoparticle Composites: Dielectric and Antibacterial Characterization

Julia Hernández-Vargas,[1] J. Betzabe González-Campos,[2] Javier Lara-Romero,[1] E. Prokhorov,[3] Gabriel Luna-Bárcenas,[3] Judit A. Aviña-Verduzco,[2] Juan Carlos González-Hernández[4]

[1]Chemical Engineering Department, Universidad Michoacana de San Nicolás de Hidalgo, Ciudad Universitaria, C.P. 58030, Morelia, Michoacán, México

[2]Institute of Chemical and Biological Researches, Universidad Michoacana de San Nicolás de Hidalgo, Ciudad Universitaria, C.P. 58030, Morelia, Michoacán, México

[3]Centro de Investigación y de Estudios Avanzados del IPN, Libramiento Norponiente # 2000, Fracc. Real de Juriquilla, Querétaro, Qro. C.P. 76230, México

[4]Biochemical Engineering Department, Instituto Tecnológico de Morelia, Avenida Tecnológico 1500, C. P. 58120, Morelia, Michoacán, México

Correspondence to: J. B. González-Campos (E-mail: JENY_MOR@yahoo.com.mx)

ABSTRACT: The dielectric and biological properties of chitosan (CTS)-based nanocomposites were analyzed by dielectric spectroscopy, and antibacterial and antifungal assays. Carbon nanotubes (CNT) and CNT decorated with silver nanoparticles (AgnP) were incorporated into a CTS matrix at different concentrations to obtain bionanocomposite thin films. The conductivity of pristine CTS is considerably enhanced, by six orders of magnitude, with the inclusion of CNT; however, with the addition of CNT decorated with AgnP it only increases by two orders of magnitude because of strong chemical interactions between the CNT and AgnP that also affect the antibacterial activity of the composite. The percolation threshold in the CTS/CNT composites is ca. 1.3 wt %, while in CTS/CNT-AgnP composites the strong CNT-AgnP chemical interactions give a percolation threshold of ca. 2.2 wt % of CNT-AgnP. In both cases, DC conductivity exhibits a three-dimensional hopping conductivity, and the σ- and α-relaxation processes are disclosed in agreement with the pristine CTS relaxation processes previously reported; however, these two relaxations vanish in the vicinity of the saturation concentration. Finally, the antifungal activity of the CTS/CNT-AgnP composites is comparable with the activity of other composites, while their antibacterial activity seems to be competitive with respect to commercial antibiotics, indicating the effectiveness of these composites in potential hygienic applications. © 2013 Wiley Periodicals, Inc. J. Appl. Polym. Sci. **2014**, *131*, 40214.

KEYWORDS: biomaterials; composites; dielectric properties; films; polysaccharides

Received 17 August 2013; accepted 19 November 2013

DOI: 10.1002/app.40214

INTRODUCTION

Polymer nanocomposites are an important class of materials that have numerous applications in a number of different industrial sectors, which is why they have been extensively studied in recent decades. Organic/inorganic nanocomposites, specifically bionanocomposites, represent an emerging group of nanostructured hybrid materials. Bionanocomposites are formed by the combination of natural polymers with organic and/or inorganic solids; they show at least one dimension on the nanometer scale. The use of bionanocomposites has been preferred because most of the synthetic polymers are not biocompatible, so natural polymers such as polysaccharides are ideal components in this type of composite material. A very attractive bionanocomposite is formed by chitosan (CTS) and carbon nanotubes (CNT); this combination is not new, and it has been studied for biosensor modification[1,2] or with a focus on its preparation, structural characterization and mechanical properties[3–9]; however, to our knowledge, there has been only one study on the dielectric properties of this composite.[10] Recently, CNT have been decorated with silver nanoparticles (AgnP) to enhance their electrical conductivity[11,12] so that they can be subsequently combined with polymers to fabricate electrically conductive polymer composites with antibacterial activity.[11,13] CTS films doped with CNT decorated with AgnP have been developed, representing an improved material for biosensor applications.[14] To the best of our knowledge, the latter is the only study regarding this combination; neither a detailed characterization about its dielectric properties nor a comparison

with CTS/CNT composites without silver decoration have been studied. Thus, the dielectric characterization of this composite is a promising topic of investigation, and it will help us understand some specific behaviors and differences between the two combinations.

In polymer nanocomposites, a complete description of the internal structural details of the conducting medium is extremely difficult due to the complex nature of the composite. The electrical conductivity depends on the microscopic and macroscopic states of the composites and gives information on the interaction of individual components inside composite material systems. Determining the electrical properties of a material is one of the most convenient and sensitive methods for studying polymer structures,[15] and knowledge of the dielectric relaxation processes in bionanocomposites is very important for their applications in different fields and for optimizing the processing parameters.

Several polymer-based composites have been investigated for their antibacterial activity. Campoccia et al.[16] reported numerous classes of antibacterial polymers as a function of the anti-adhesive polymer coating: poly(ethylene oxide) (PEO), poly(ethylene glycol) (PEG), or polyacrylamide, and polymers with intrinsic antibacterial properties, i.e., CTS derivatives and polycationic polymers such as arginine or bioactive glass materials and alloys containing antibacterial metals. In addition, they reported a list of nonantibiotic antimicrobial drugs associated with different biomaterials that have been used as delivery systems for a given substance, for example, metallic nanoparticles, peptides and functionalized polyanilines (fPANI). In this way, Gizdavic-Nikolaidis et al.[17] investigated the antimicrobial properties of conductive fPANI by exploring their interactions with bacterial cells, and Gizdavic-Nikolaidis et al.[18] suggested that the length of the polymer chain could also contribute to the antibacterial activity. As can be observed, polymer-based composites with biological activity are currently of great interest because of their potential uses in different applications were hygiene is a key factor.

The antibacterial and antifungal activities of CTS and CTS-based composites are well known, and more recently, Gonzalez-Campos et al.[19] proposed a method that correlates electrical properties to antibacterial activity. They found that the percolation threshold concentration of this composite correlates well with the maximum of bactericide activity, and therefore, the percolation effect might help to explain the observed maximum bactericide activity of CTS/AgnP composites. It also seems that the mechanism by which CTS exerts some of its effects on the anionic cell membranes resembles the mechanism of other potential antibacterial conducting polymers such as (fPANI).[17]

Because of the results described above, the aim of this work is to investigate the dielectric relaxation properties of the CTS/CNT and CTS/CNT-AgnP biocomposites to gain a better understanding of the nature of their molecular dynamics and their dielectric properties. Additionally, the antibacterial and antifungal activity of both combinations was evaluated to examine if there is a relationship between the electrical properties and the biological activity of these composites.

MATERIALS AND METHODS

CNTs were synthesized by the spray pyrolysis process; a vycor tube was attached to a pneumatic device used as a solution atomizer. The overall tube dimensions were 0.9 cm internal diameter and 23-cm length. A cylindrical furnace (Barnstead, Thermolyne 1200, California) equipped with a high precision temperature controller (±1 K) was used to achieve the desired reaction temperature. α-Pinene (Aldrich, 98.00%) was used as the carbon source. For the synthesis, 25 mL of the selected carbon feedstock and 1.00 g of ferrocene (Aldrich, 98.00%) were placed in a glass container and carried through the pneumatic device with Argon (99.99%, Praxair) at an 83.33 cm^3/s flow rate for 30 min at 800°C. The multiwalled carbon nanotube (MWCNT) films produced during each reaction at the inner surface of the vycor tubing were removed from the vycor substrate to be purified and functionalized by a conventional acid treatment to achieve their dispersion in water. Silver nanoparticles were supported on the MWCNTs by the microwave method. Silver nitride (Aldrich, 99.99%) was used as a metal source; dioctyl sodium sulfosuccinate (AOT) was used as a surfactant, and $NaBH_4$ was the reducing agent. The microwave method was performed in a Synthos 3000 microwave reactor (Anton-Parr) at 120°C for 15 min. The produced MWCNTs and composites were characterized by HRTEM, Raman spectroscopy and thermogravimetric analysis (TGA).

The TEM micrographs were obtained using a Philips CM-200 analytical (TEM) operating at 200 kV. The TEM specimens were prepared by dispersing them in acetone and sonicating for 2 min. A drop of the suspension was placed on a perforated carbon coated Cu grid and allowed to dry. Raman spectroscopy was performed using a Labram system model Dilor micro-Raman equipped with a 20 mW He-Ne laser emitting at 632.8 nm and a holographic notch filter made by Kaiser Optical Systems, Inc. (model supertNotch-Plus) with a 256 × 1024-pixel charge-coupled device (CCD) used as the detector. All measurements were carried out at room temperature with no special sample preparation.

CTS/CNT and CTS/CNT-AgnP Films Preparation

CTS of medium molecular weight (M_w = 150,000 g/gmol) with an 82% degree of deacetylation, as reported by the supplier, and silver nitrate (99.99% trace metal basis) were purchased from Sigma–Aldrich. Acetic acid from Baker was used as received. CTS/CNT films were obtained by dissolving 1 wt % of CTS in a 1 wt % aqueous acetic acid solution with subsequent stirring to promote dissolution. This solution was poured into a Petri dish, and the water was allowed to evaporate at 60°C to obtain a pristine CTS film. The corresponding amount of CNT or CNT-AgnP powder (0.5, 1, 1.5, 2, 3, 4, 5, and 8% w/w respect to the weight of CTS dry film) was poured into a 1 wt % aqueous acetic acid solution and further sonicated for 30 min to obtain the nanotube or nanotube/nanoparticle solution. The silver content in the CNT-AgnP powder was estimated to be ~20% wt %. Afterward, the pristine CTS film previously prepared was dissolved into the CNT or CNT-AgnP solution and further sonicated for 10 min to eliminate bubble formation. CTS/CNT and CTS/CNT-AgnP films were prepared by the solvent cast method

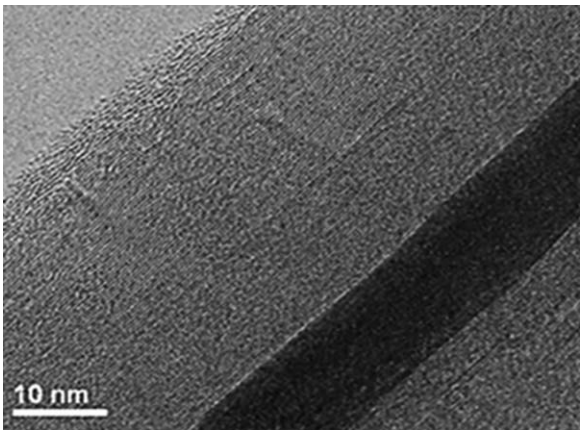

Figure 1. HR-TEM image of synthesized CNTs.

by pouring the final solution into a plastic Petri dish and allowing the solvent to evaporate for 24 h at 60°C. A thin layer of gold was vacuum deposited onto both film sides to serve as electrodes. Rectangular small pieces (5 mm × 4 mm) of these films were prepared for measurements.

The free water content of the films was determined by thermogravimetrical analysis on Mettler Toledo apparatus, model TGA/SDTA 851e, using an aluminum sample holder under argon atmosphere with a flow rate of 75 mL/min. The amount of free water may be evaluated by the decrease in sample weight during the heating scans with a heating rate of 5°C/min. The sample masses ranged from 5 to 10 mg with no special preparations required.

Infrared Measurements and Morphology Analysis

The chemical analysis of CTS/CNT and CTS/CNT-AgnP composites was performed by FTIR on a Perkin–Elmer spectrophotometer using an ATR accessory in the 4000–650 cm^{-1} range. The resolution was set to 4 cm^{-1}, and the spectra shown are an average of 32 scans.

Dielectric Measurements

Dielectric measurements were carried out using an Agilent Precision Impedance Analyzer 4294A operating at a 100 Hz to 110 MHz frequency range. The amplitude of the collected signal was 100 mV. A peltier and a resistance heating element were used to perform measurements from 2 to 250°C. Each sample was left at each measured temperature for 3 min to ensure thermal equilibrium. Triplicate measurements were performed to verify repeatability.

Antimicrobial Assay

The antimicrobial susceptibility of silver nanoparticles was evaluated using the disc diffusion *Kirby-Bauer* method.[20] Two bacteria and two fungi were used in this study. *Escherichia coli* and *Streptococcus aureus* were used as model Gram-negative and Gram-positive bacterium, respectively, and the fungi tested were *Saccharomyces cerevisiae* (YSH1170) and *Debaryomyces hansenii* (PYC2968). Commercial antibiotics: ampicillin, cephalothin, cefotaxime, dicloxacillin, clindamycin, ciprofloxacin, erythromycin, tetracycline, vancomycin, sulfamethoxazole, and trimethoprim were used as bacteria controls, and ketoconazole and miconazole in ethyl acetate were used as controls for fungi.

RESULTS AND DISCUSSION

CNT Synthesis

Figure 1 is an HR-TEM image of the CNT produced by the method described above. MWCNTs with ~88 walls, a 69 nm external diameter and a 7.8 nm internal diameter were produced. The FTT image analysis (not shown) indicates that the interplanar distance is ~0.335 nm. The high alignment walls and the homogeneous spacing suggest a high crystallinity of the CNT. According to TGA measurements (not shown), the purity of the CNT synthesized in this work is ~96.08%.

Figure 2(a) shows the HR-TEM image and EDAX analysis from which it can be confirmed that the CNTs were decorated with silver nanoparticles by the microwave method, using AOT as the surfactant and $NaBH_4$ as the reducing agent. It can be observed that silver nanoparticles are discretely dispersed on the CNT surface. The histogram of the size distribution is shown in Figure 2(b).

CTS/CNT and CTS/CNT-AgnP Films

The solvent cast method used for the CTS/CNT and CTS/CNT-AgnP nanocomposite films synthesis allows the formation of

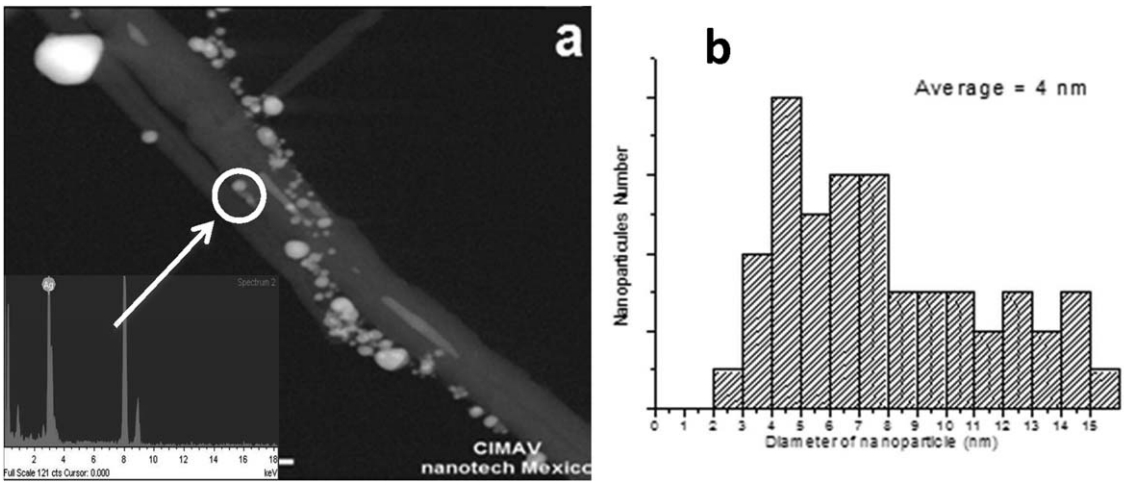

Figure 2. (a) HR-TEM image of CNT decorated with silver nanoparticles and EDAX analysis and (b) nanoparticle size distribution histogram.

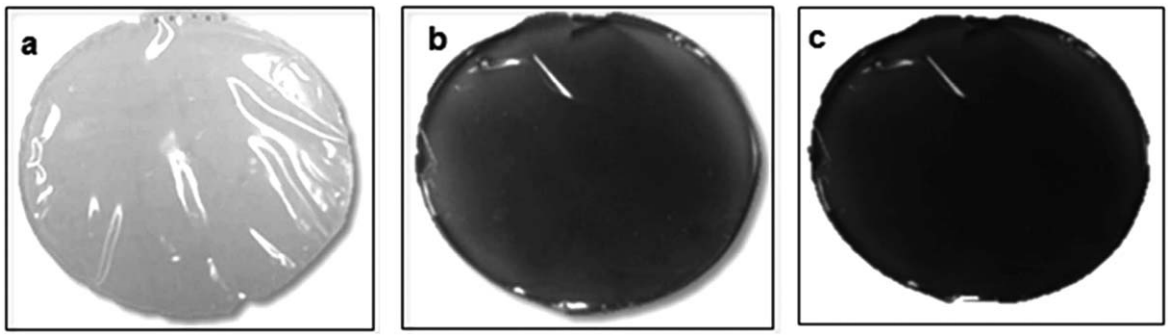

Figure 3. (a) Pristine CTS film, (b) CTS/CNT-AgnP 1 wt % film, and (c) CTS/CNT-AgnP 3 wt % film.

self-supported, stable, and flexible cellophane-like appearance films, ~30-μm thick. As it is shown in Figure 3, a change from transparent to gray, dark gray and black ascribed to the presence of CNT or CNT-AgnP is noticeable when compared with pristine CTS films. The amounts of CNT and CNT-AgnP were 0.5, 1, 1.5, 2, 3, and 4 wt %.

FTIR Analysis

The Infrared spectra of pristine CTS, CTS/CNT and CTS/CNT-AgnP (0.5, 1, 3, and 4 wt %) composites are shown in Figure 4(a,b). It can be observed that nanocomposites with 3 wt % of CNT-AgnP show a clear difference from pristine CTS, specifically in the stretching and bending vibration bands

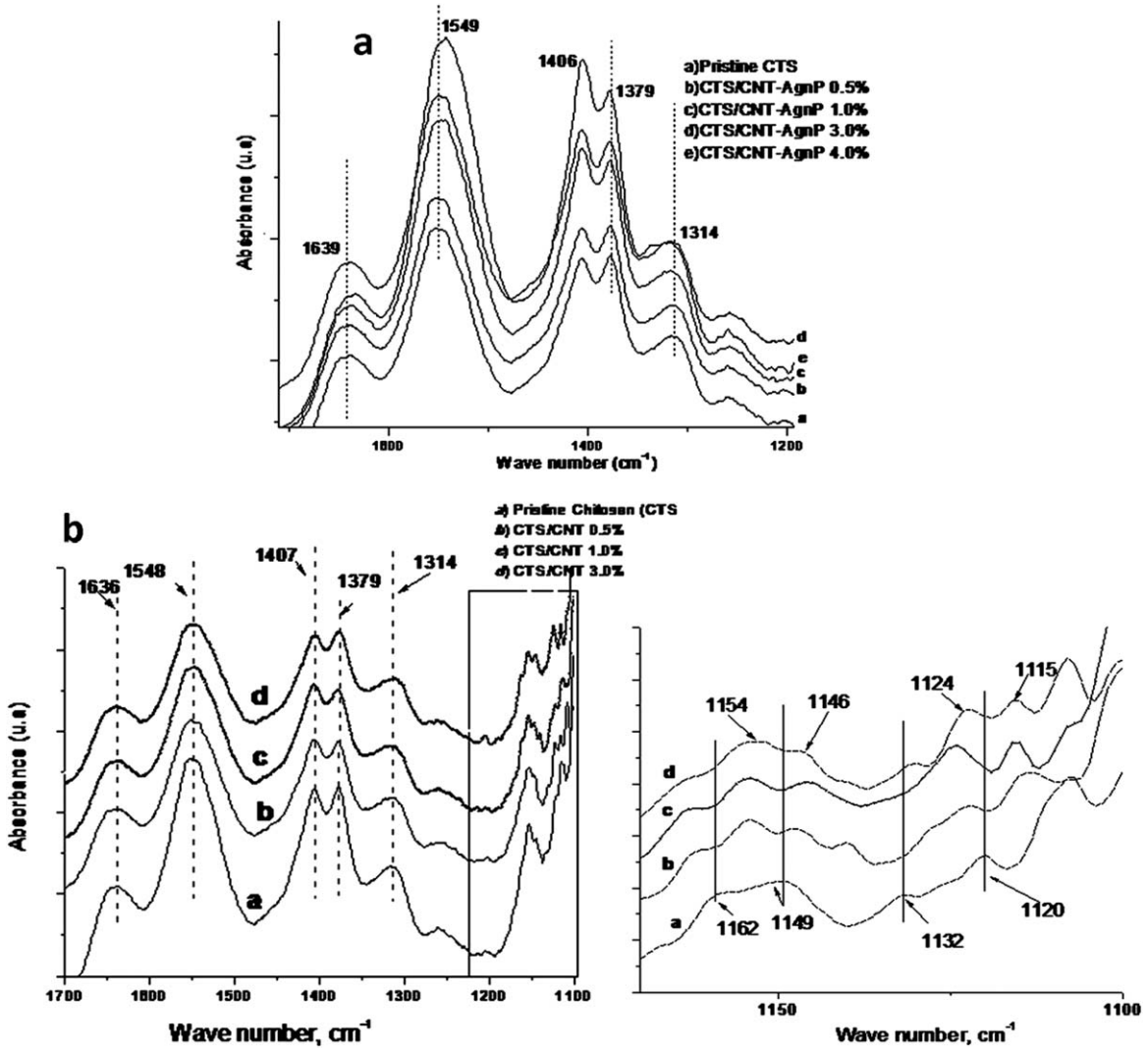

Figure 4. FTIR spectra of (a) CTS/CNT-AgnP composites and (b) CTS/CNT composites.

corresponding to the amine, amide and hydroxyl groups; the characteristic peaks at 1639 cm^{-1} (amide I group), 1549 cm^{-1} (bending vibrations of NH_2), 1379 cm^{-1} (amide III), and 1314 and 1259 cm^{-1} bands (OH bending vibrations) show a slight shift to lower wave numbers, indicating interactions between these functional groups and the filler. However, this case does not hold for 0.5 and 1 wt % nanocomposites. As can be observed in Figure 4(a,b), at these low concentrations, there is no evidence of chemical interaction between the $CONH_2$, NH_2, and OH hydrophilic groups of CTS, given that their corresponding vibration bands do not change their position or intensity. This result indicates that at least 3 wt % CNT-AgnP filler with respect to the dry weight of CTS is needed to demonstrate chemical interactions between the components; this amount represents ~0.6 wt % of AgnP and 2.4 wt % of CNT (the weight percent of AgnP in CNT-AgnP powder is estimated to be ~20%). The shift of these characteristic vibrations to lower wave numbers is proportional to the weight percent of the filler, in agreement with previous reports on the CTS/AgnP composite with commercial silver nanoparticles mechanically incorporated into the CTS matrix,[21] where a very significant shift (in some bands up to 20 cm^{-1}) of IR bands is observed in the CTS/AgnP composites with 1, 3, 5, and 10 wt % of AgnP with respect to the pristine CTS IR spectrum. In addition to the higher concentration of silver nanoparticles compared with the one presented here, this larger shift could also be related to the larger size of commercial nanoparticles used in the previous work (25 nm for the CTS/AgnP composite versus ~4 nm in this case).

Special mention should be made of the band observed at 1406 cm^{-1}; this band has been related to the antimicrobial character of CTS in the literature,[21] and the change in intensity of this band related to the CTS-based films' antimicrobial testing has recently been reported.[22] In the CTS/CNT-AgnP composites shown in Figure 4(a), it is evident that at concentrations of the filler above 1 wt %, this band is always higher than the one at 1389 cm^{-1}, which is not the case for CTS/CNT composites [see Figure 4(b)]. From these results, it seems that the presence of silver nanoparticles tends to enhance the antimicrobial activity of CTS. These results will be discussed below in relation to the antimicrobial activity.

On the other hand, for the CTS/CNT bionanocomposites [Figure 4(b)], there is no evidence of chemical interaction among the $CONH_2$, NH_2, and OH groups of CTS and CNT, as the characteristic bands of these groups remain unchanged. This result leads us to the conclusion that these groups of CTS interact chemically only if silver nanoparticles are present. In this case, the interaction between CTS and CNT is different: the IR band at 1149 cm^{-1} assigned to the special broad peak of the β(1–4) glucosidic band in a polysaccharide unit that changes into a doublet at 1154 cm^{-1} and 1146 cm^{-1}, revealing that the C—O—C groups in the glucose ring interact with CNT via weak interactions and thus confirming the formation of the CTS–CNT nanobiocomposites. The same phenomenon happens with the vibration band at 1120 cm^{-1} corresponding to the C—O—C and C—O vibrations dominated by ring vibrations in various polysaccharides. The appearance of two new bands at 1154 cm^{-1} and 1115 cm^{-1} is ascribed to the interaction of carboxylic

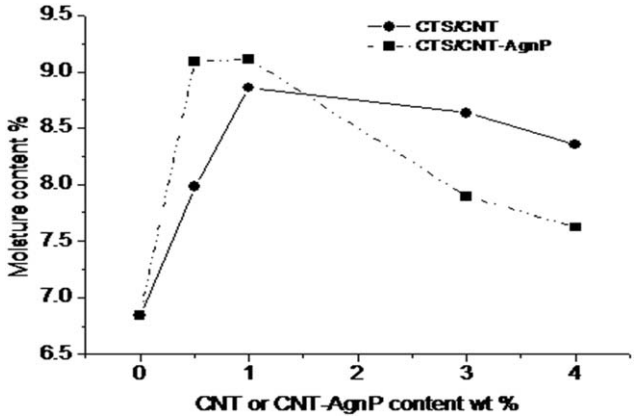

Figure 5. Moisture content of pristine CTS, CTS/CNT films, and CTS/CNT-Ag films as a function of the wt % of the filler.

groups of CNT and hydroxyl groups of CTS that originate these bending vibrations of C—O—C groups due to the formation of ester bonds. It is important to note that this case does not hold for CTS/CNT-AgnP composites; therefore, the inclusion of AgnP to CNT inhibits the interaction between CNT and CTS, and there is no formation of ester bonds; this fact therefore supports a strong chemical interaction between AgnP and CNT.

Thermogravimetric Analysis

The moisture contents of the CTS/CNT and CTS/CNT-AgnP bionanocomposite films were determined by thermogravimetric measurements and are shown in Figure 5. There is a slight difference in the water content at different concentrations in both composites. The lowest moisture content is for pristine CTS films, increasing as the weight percent (wt %) of the fillers (CNT or CNT-AgnP) increases up to 1 wt %. However, in both cases, above 1 wt % filler, the moisture content decreases, more evidently in the CTS/CNT-AgnP films. It is well known that the functionalization of CNT is an effective way to prevent nanotube aggregation; it yields a better dispersion and stabilizes the CNT within a polymer matrix. Carboxylic and hydroxyl groups are polar groups and can take part in hydrogen bond formation, so these groups attached to CNTs give them a hydrophilic character.

As can be observed in Figure 5, the incorporation of low quantities of CNT-AgnP (i.e., below 1 wt %) into the CTS matrix significantly increases the hydrophilic character of the biopolymer. As shown by FTIR analysis, at concentrations below 1 wt % of the filler, there is no evidence of chemical interaction between the CTS hydrophilic groups and CNT-AgnP, and therefore, both components preserve and combine their capacities to bond with water through hydrogen bonds, increasing the moisture content in composite films. However, above this concentration, the moisture absorption capacity decreases as the AgnP content increases, which is in agreement with the incorporation of commercial silver nanoparticles into the CTS matrix,[23] where at concentrations of 1 wt % of AgnP and above, the moisture content decreases as the wt % of AgnP increases. This result is ascribed to the chemical interaction of the hydrophilic groups of CTS and silver nanoparticles that leads to the formation of a polymeric composite structure.[23]

On the other hand, it has been suggested that CNT are wrapped by CTS,[24] and therefore, as the CNT concentration increases, the possibility of an interaction between the hydrophilic groups of CTS and functionalized CNT is lower. This effect is responsible for the production of polymeric composite structures with nanotubes, which decreases the water absorption ability of the composites as the CNT content increases. It is noteworthy that the CTS/CNT-Ag films with concentrations above 1 wt % show slightly higher moisture content with respect to CTS/CNT films. It was shown in the IR analysis that CNT does not interact with hydrophilic groups of CTS, and therefore, these groups are available to link with water, resulting in a higher water absorption capacity compared with CTS/CNT-Ag composites.

Dielectric Measurements

In general, the electrical conductivity of composites depends on the microscopic and macroscopic states of the composites and provides information on the interaction of individual components inside composite material systems. In a mixture between a dielectric and a conducting component, the conductivity of this mixture shows a critical behavior if the fraction of the conducting component reaches the percolation threshold.[25]

The DC conductivity of the composites was obtained from the extrapolation of impedance measurements to zero frequency, as previously described[10,26,27] and using the dimensions of each film. The DC conductivity of pristine CTS, CTS/CNT, and CTS/CNT-AgnP films at 25°C is shown in Figure 6. It is noteworthy that neat CTS exhibits low ionic conductivity, which can be related to the presence of small concentrations of conductive species in the form of NH_3^+ groups and H^+ ions.[26] A significant increase in the CTS conductivity is observed with the inclusion of the fillers; in CTS/CNT composites, the conductivity increases as CNT wt % increases up to 3 wt %, where the conductivity enhancement is greater than five orders of magnitude. Above this concentration, the conductivity monotonously increases with the wt % of CNT. This conductivity augmentation has been observed in previous reports on macro porous CTS/CNT scaffolds[28] and CTS/CNT fibers[29] where the percolation threshold was 3 wt % of CNT.

In CTS/CNT-AgnP composites, the increase in conductivity compared with pristine CTS is approximately three orders of magnitude; this increment is comparable to the results reported for a CTS/AgnP composite.[23] This lower conductivity compared with the CTS/CNT composite may be a consequence of the Ag-CNT chemical interaction (see FTIR analysis). An enhanced conductivity within the sample as a result of increasing the number of mobile charge carriers and a synergistic effect of CNT and AgnP was expected; however, this case does not hold. As shown by FTIR analysis, there is a strong interaction between CNT and AgnP that could be hindering charge carriers mobility and leads to no substantial change in conductivity below 2 wt %, in contrast to expectations. Previous XPS (X-ray photoelectron spectroscopy) analysis of CTS/AgnP composites[19] indicates the presence of Ag^+ ions by the appearance of two new peaks. These silver ions interact with the amine and hydroxyl moieties in CTS and are in turn a driving force for ionic conduction that could change DC conductivity in bionanocomposites; however, higher concentrations compared with CS/CNT composites are needed to increase the conductivity of CS/CNT-AgnP composites. Potara et al.[30] indicates that CTS confers a positive change on AgnP, thus increasing the conductivity of composites; nonetheless, the interaction between AgnP and CNT interferes in this process, directly affecting the conductivity of composites.

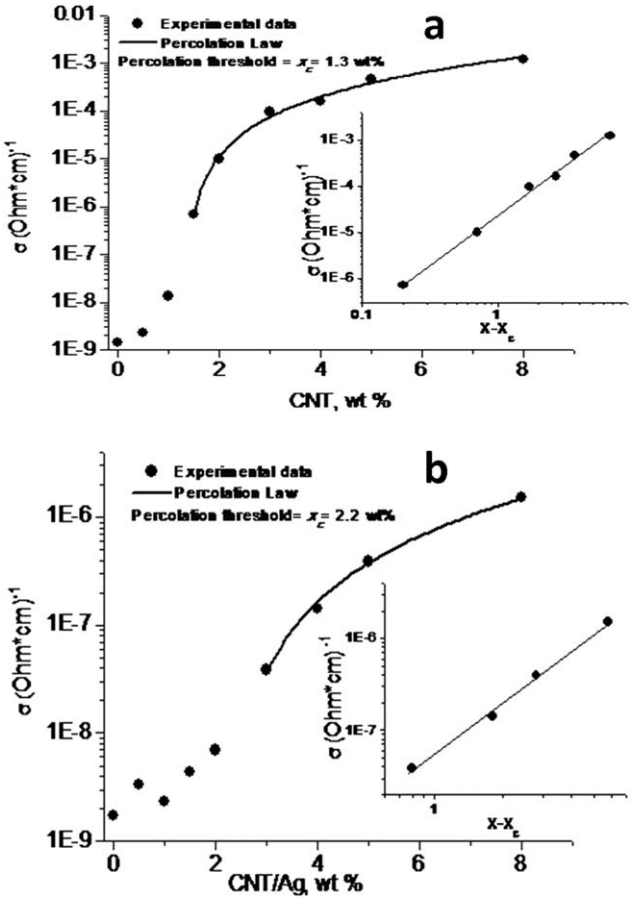

Figure 6. Room temperature (25°C) DC conductivity of CTS/CNT (a) and CTS/CNT-AgnP (b) composites as a function of filler content.

When metallic fillers are dispersed in an insulating matrix, percolation theory predicts that the DC conductivity of the composite in the vicinity of the percolation threshold varies as follows[31]:

$$\sigma\alpha(x-x_c)^t \quad (1)$$

where x is the weight percent of the conductive phase; x_c is the critical concentration at the percolation threshold; and t is a critical exponent that depends only on the dimensionality of the percolation system with values typically at 1.3 and 2.0 for two and three dimensions, respectively.[32] This dependence produces a straight line with a slope equal to t in a double log–log plot of the electrical conductivity versus $x - x_c$ as shown in the window inset of Figure 6.

In our case, the percolation threshold indicates that the nonconducting—conducting state transition takes place in the CTS/CNT composite at ca. 1.3 wt %, which was calculated by fitting

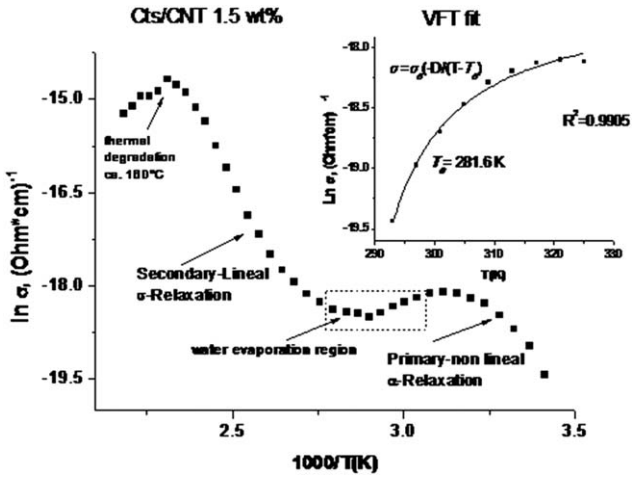

Figure 7. ln σ_{DC} versus 1000/T (K) for CTS/CNT 1.5 wt % composite film.

the experimental data to eq. (1) [Figure 6(a), continuous line], while for CTS/CNT-Ag, the composite percolation threshold is 2.2 wt %. The percolation threshold is a critical value that is due to formation of the conductive path. At this value, the conversion of insulator to conductor will occur. Low x_c values have been encountered in systems where the conducting phase is inhomogeneously distributed along the paths running from one electrode to another.[33] It has been demonstrated that in CTS/AgnP composites, the antibacterial activity is directly related to the percolation threshold concentration determined by conductivity measurements[19]; therefore, in this instance, it is also possible to analyze the composites studied herein in this regard.

On the other hand, the critical exponents (t) for CTS/CNT and CTS/CNT-AgnP composites are $t = 2.08 \pm 0.06$ and 1.87 ± 0.08, respectively. These values imply that both systems are three-dimensional according to the well-established values.[32] This result is in agreement with previous reports on composite containing CNTs.[34] In contrast, when CTS is combined with AgnP only, these composites exhibit a two-dimensional hopping conductivity with a critical exponent t of 1.32.[35] This result indicates that the presence of CNT in composites leads to 3D conductivity systems.

Figure 7 shows the ln σ_{DC} versus temperature dependence for a 1.5 wt % CTS/CNT nanocomposite calculated at zero frequency according to González-Campos et al.[26] This conductivity trend is the typical behavior of pristine wet-CTS and wet CTS/AgnP composite films[23,27,35]; the nonlinear α-relaxation can be clearly observed. This process corresponds to the segmental relaxation associated with the glass rubber transition temperature, T_g, at which the micro-Brownian motion of a long chain segment in the amorphous phase of CTS takes place, where relaxation is followed by the water evaporation region, characterized by almost no change in conductivity.[23,27] The Arrhenius type σ-relaxation process is associated with the hopping motion of ions in the disordered structure of the biomaterial,[36] and finally the thermal degradation above 160°C.[28] It is important to note that this typical behavior observed in Figure 7 and described above was disclosed exclusively in samples with CNT-wt % below 1.5 wt % CNT (i.e., 0.5, 1.0, and 1.5 wt %), whereas in samples with higher CNT contents, the conductivity trend is almost constant (see Figure 8). This feature distinguishes systems above the percolation threshold (remember that the percolation threshold for CTS/CNT composite was ca. 1.3 wt %).

On the other hand, from Figure 8, it can also be observed that the thermal degradation of pristine CTS is not modified regardless of the filler's concentration. However, the water evaporation region is more evident in CTS/CNT composites because of the different interactions with water compared with pristine CTS, which modifies the starting temperature for the σ-relaxation being higher for CTS/CNT composites.

The nonlinear α-relaxation can be well described by the Vogel–Fulcher–Tammann (VFT) relationship, $\sigma_{dc} = \sigma_0 \exp\left(-\frac{D}{T-T_0}\right)$, where σ_0 is the pre-exponential factor; D is a material constant; and T_0 is the so-called Vogel temperature related to the glass transition temperature.[37] From the fitting of the experimental data to this model (as shown in the window inset of Figure 7), T_0 can be calculated and the glass transition temperature (T_g) can be assigned as previously described[27,37] (where T_0 is 50 K below T_g). It is noteworthy that in CTS/CNT nanocomposites, the calculated Vogel temperature increases as the CNT concentration increases (not shown). Although there is a slight difference in the water content of the composites (see Figure 5), which in turns could be affecting their Vogel temperature, the effect of the weight percent of the CNT on the Vogel temperature is stronger than the water content's effect as a result of the restricted motion of the main chains because of the chemical interaction between CTS and CNT. It is important to note that this calculation can only be performed on samples that show the appropriate behavior region (e.g., CTS with 0.5, 1, and 1.5 wt % CNT).

The metallic type conduction is evident in CS-CNT at concentrations of CNT greater than 1.5 wt %, as seen in Figure 8. This event can also be observed in the dielectric modulus versus frequency dependence as is shown in the window inset of Figure 9 (only selected temperatures are shown). The complex modulus

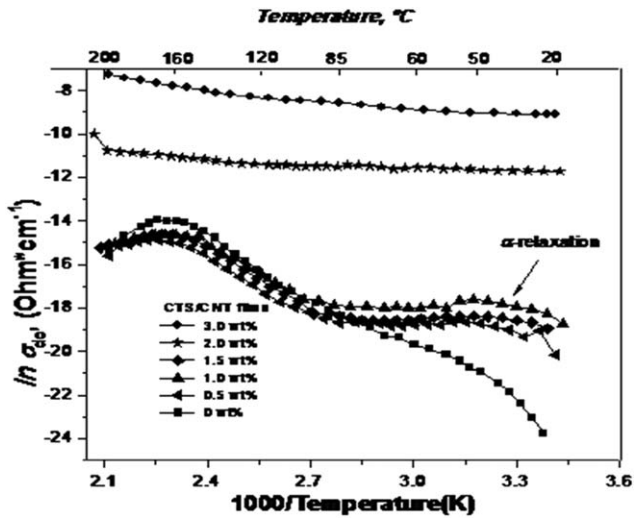

Figure 8. ln σ_{DC} versus 1000/T (K) for CTS/CNT composites.

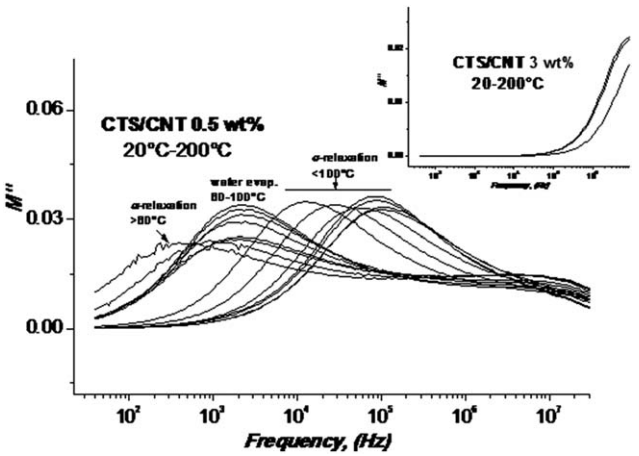

Figure 9. Dielectric modulus versus frequency dependence for CTS/CNT 0.5 wt % composite. Window inset: Dielectric modulus versus frequency for CTS/CNT 3 wt % composite.

$M^* = M' + jM''$ is the reciprocal of the permittivity ($M^* = j\omega C_0 Z^*$), which is a very useful and convenient tool to analyze and interpret the dielectric relaxations of polymeric materials, as by this formulism the electrode polarization effect can be suppressed.[38] This formulism corresponds to the relaxation of the electric field in the material when the electric displacement remains constant; therefore, the electric modulus represents the real dielectric relaxation process. Because the electrode effect is very important in CTS systems,[26,27] we have analyzed the dielectric spectrum by M'', which can be determined from the following relations[38]:

$$M' = \omega C_0 Z'', M'' = \omega C_0 Z'$$

where M' and M'' are the real and imaginary parts of the dielectric modulus, respectively, and C_0 is the vacuum capacitance given by $\varepsilon_0 A/t$, where t is the thickness, A is the area of the film, and ε_0 the permittivity of free space, which has the value $8.854\ 187 \times 10^{-12}$ ($F \times m$). The value ω is the angular frequency that is equal to $\omega = 2\pi f$, and f is the frequency of the applied field.

Figure 9 shows the imaginary part of the dielectric modulus (M'') versus the frequency at selected temperatures from 20 to 200°C for a CTS/CNT 0.5 wt % wet-film; the change from the α-relaxation process below 60°C to the water evaporation region between 60 and 100°C (where peaks frequency is almost constant) and later, above 100°C, to the thermally activated σ-relaxation process, is clearly observed. The σ-relaxation peaks shift toward the higher frequency side with increasing temperature, as the motion of the polymer chains increases due to the increase in temperature; the accumulation of the free charges occur at the interface within the sample. Additionally, there is an increase in the charge carrier mobility. As a result, the relaxation time decreases, and there is a shift of the loss peak toward the higher frequency side with increasing temperature. The processes associated with these peaks should obey the Arrhenius dependence, according to Figures 7 and 8. However, such is not the case for CTS/CNT films with CNT contents above 1.5 wt %; as shown in the window inset of Figure 9, from 20 to 200°C the dielectric modulus does not reveal any peaks as evidence of the α or σ relaxation processes previously mentioned, as these concentrations are above the calculated percolation threshold (1.3 wt %). This indication of saturation agrees with Figure 6(a).

From the M'' peaks disclosed in the wet films (Figure 9), the transitions from one relaxation process to another as the temperature rises can be clearly observed, and it might even be possible to differentiate wet from dry films. In the case of dry films of CTS-based composites, the M'' versus temperature dependence shows no peaks related to the α-relaxation or water evaporation; only peaks belonging to the σ-relaxation process are observed.[35] Similarly, from this dependence, it is possible to calculate the relaxation time and, as a result, the activation energy of this relaxation process. The corresponding relaxation is time $\tau_\sigma = 1/(2\pi v_p)$, where v_p is the peak frequency of M'' at each temperature.[39] For the σ-relaxation process, the relaxation time shows an Arrhenius type dependence, and the slope is the activation energy for the process. In these composites, the calculated activation energies of the composites are between 80 and 83 kJ/mol, and these values correlate well with the values obtained by fitting the complex permittivity in CTS/AgnP composites using the Havriliak-Negami model.[23,27] This linear behavior was also observed above 70°C in wet CTS/AgnP composite films, and according to the dielectric and DMA results, it does not depend on moisture content.[23]

The ln σ_{DC} versus $1000/T$ (K) dependences for CTS/CNT-AgnP nanocomposites are shown in Figure 10. The same behavior described above for wet CTS/CNT composites and previously described for wet CTS/AgnP composites[23] is observed; i.e., the α-relaxation, the water evaporation, the σ-relaxation and finally the thermal decomposition above 160°C (not shown). This dependency was observed in composites with filler contents below 3 wt %. As observed in the CTS/CNT composites, for 3 and 4 wt %, no relaxation processes are revealed in the ln σ_{DC} versus temperature dependencies for these concentrations (see Figure 10), and only thermal degradation is clearly observed. Thermal degradation does not change with varying the concentration of the filler, in contrast to the CTS/AgnP composite films previously reported, where thermal stability increases by ~20°C compared with pristine CTS films.[23] On the other hand, the Vogel temperature increases as the CNT-AgnP content increases (see window inset of Figure 10); the opposite was true of CTS/AgnP composite films.[23] It was established that in CTS/AgnP composite, the addition of AgnP screens the CTS-CTS interactions and facilitates segment motion, leading to lower glass transition temperatures as the wt % of AgnP increases[23]; however, in the case of CTS/CNT-AgnP composites, the chemical interaction between CNT and AgnP described above eliminates this possibility, and the incorporation of the fillers in the polymer matrix increases the glass transition temperature due to the hindered chain and segmental mobility of the polymers.

The water evaporation region is more evident in CTS/CNT-AgnP composites than in pristine CTS. This water evaporation region masks the thermally activated σ-relaxation process in this temperature region, but it is possible to avoid this masking if an annealed pretreatment is performed to obtain dry samples.[23,27]

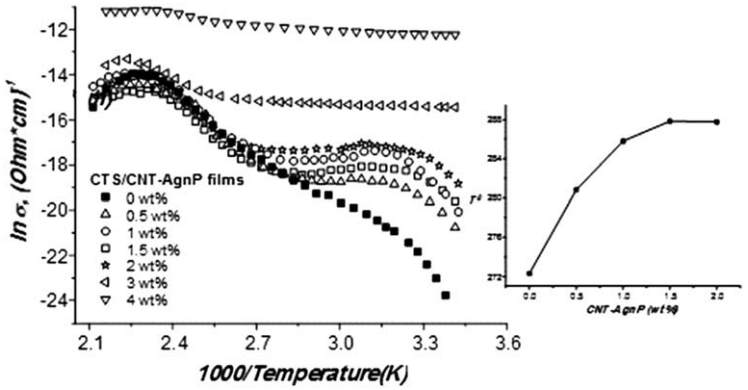

Figure 10. ln σ_{DC} versus 1000/T (K) for CTS/CNT-AgnP composites. Window inset: Vogel temperature versus CNT-AgnP content.

Bacteriological Analysis

The antibacterial activity of the three components that make up the composites presented here is well known[19,30,40–43] and a source of great commercial potential: the antibacterial activity of CTS and its composites has been attracting substantial attention from researchers. Recently, Gonzalez-Campos et al.[19] have proposed a method that correlates electrical properties with antibacterial activity. They found that the percolation threshold concentration of this composite correlates well with the maximum bactericide activity.

In this regard, CTS/CNT and CTS/CNT-AgnP composite films were tested for their antibacterial activity using the disc diffusion method.[20] *Escherichia coli* was used as a model Gram-negative bacterium and *Streptococcus aureus* as a model Gram-positive bacterium. The CTS/CNT and CTS/CNT-AgnP composite film contents tested were 0.5, 1, 1.5, 3, 4, 5, and 8 wt % of either CNT or CNT-AgnP with respect to the CTS weight. They were cut into discs of 1 cm diameter, UV sterilized for 24 h and placed in the Moller-Hilton agar where the model bacteria were previously cultivated. The agar plates were then incubated for 24 h at 37°C, and the inhibition zone was measured directly for each specimen and each bacteria species.

Figure 11(a) shows the antibacterial activity results. The graph shows the bactericide efficiency of the CTS/CNT and CTS/CNT-AgnP composite discs. There is a similar trend in both composites, and the highest inhibition efficiency against *E. coli* was obtained with 0.5 wt % regardless of the filler. The inhibition diameter changed from 11 mm for pristine CTS to 15 mm and 13 mm for CTS/CNT and CTS/CNT-AgnP, respectively. It can be observed that in the case of the Gram-negative bacteria, CNT are slightly more effective than CNT decorated with AgnP, while for the Gram-positive bacteria *S. aureus* [Figure 10(b)], the best result was with the CTS/CNT-AgnP 1 wt % composite, in which case the diameter changed from 14 to 16 mm in comparison to pristine CTS.

From the results in Figure 11, it can be observed that the CTS/CNT-AgnP 1 wt % composite shows the best performance against Gram-positive bacteria. As shown by FTIR analysis, above this concentration of filler, there are chemical interactions between CNT and AgnP that in turn could affect the antibacterial activity. The enhanced antibacterial activity of CTS films with the inclusion of silver nanoparticles has been previously reported.[19,30,40] This antibacterial activity increases as the load of silver nanoparticles increases until it reaches a maximum at a critical concentration that correlates well with the percolation threshold concentration determined by conductivity measurements.[19] Therefore, the percolation effect could help explain the observed maximum bactericide activity of CTS/AgnP composites. Nevertheless, in these cases, there is not a clear relationship between the electrical properties of the composites and their antibacterial activity. However, the maximum bactericide activity observed in the CTS/CNT composite against *S. aureus*

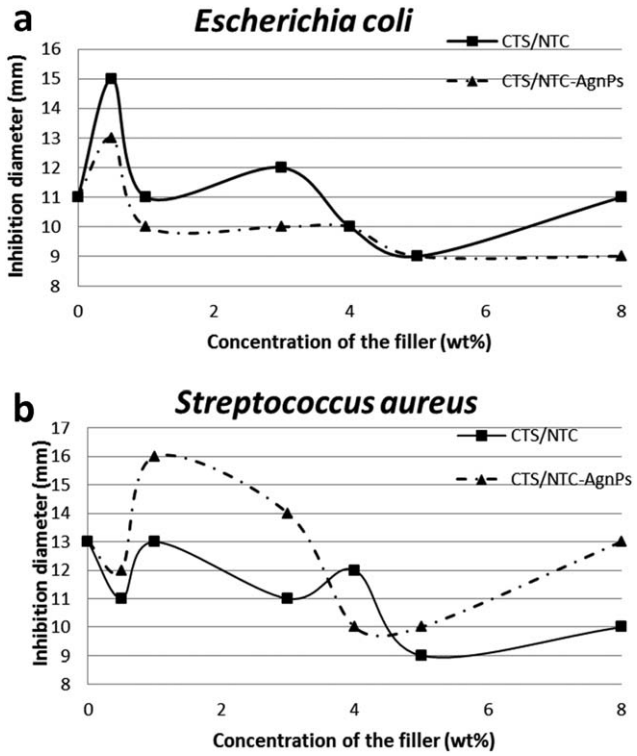

Figure 11. Microbiological analysis of each material, graphically evaluated (a) for *E. coli* and (b) for *S. aureus*.

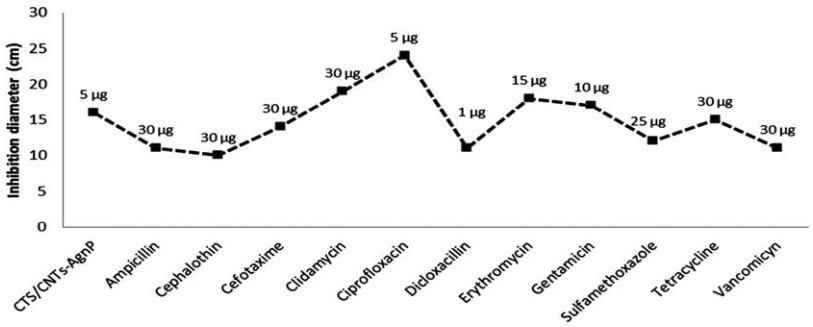

Figure 12. Commercial antibiotics compared with CTS/CNTs-AgnP 1% wt. composite against *S. aureus* bacterium.

is near the percolation threshold concentration (1.3 wt %) [see Figure 11(b)].

In the presence of MWCNT, direct cell contact seriously impacts the cellular membrane's integrity, metabolic activity and morphology in *E. coli*, and the bacterium endures stresses related to cell membrane damage and oxidative stress.[42] In CTS/CNT composites, there is a distinct possibility that strong hydrogen and ester bonds may form between CTS and CNTs (see FTIR results). Consequently, this compatibility and strong interaction between CNT and the matrix could affect the individual antibacterial activity of each component, reducing the possibility of interactions with the cell membrane, especially at filler concentrations above 1 wt %, according to the FTIR results presented above.

On the other hand, CTS may prevent silver nanoparticle agglomeration below a critical concentration[19] and confer a positive charge to nanoparticles, enhancing their binding to the negative charges present at the cell surface.[19,30] The antibacterial mechanism of silver ions has been related to their interaction with the thiol group of cysteine in the cell membrane of bacteria[42] while AgnP may attach to the surface of the cell membrane disturbing permeability and respiration functions of the cell or even penetrate it.[43] In CTS/AgnP composites, a synergistic effect of CTS with silver ions and metallic silver nanoparticles is responsible for the higher antibacterial properties of this composite.[19]

As mentioned above regarding the FTIR analysis, the band arising at 1406 cm^{-1} had been previously related to the antimicrobial character of CTS in the literature.[21] In the FTIR spectra of the CTS/CNT-AgnP composite [Figure 4(a)], it is evident that at concentrations of the filler above 1 wt %, this band is always higher than the one at 1389 cm^{-1} [which is not the case for CTS/CNT composites, see Figure 4(b)]. From these results, it seems that the presence of silver nanoparticles enhances the antimicrobial activity of CTS for a filler content above 1 wt %. However, in the CTS/CNT-AgnP composite, the antibacterial activity is strongly affected by the chemical interaction between CNT and AgnP shown above by FTIR, especially at concentrations above 1 wt % of the filler; this affinity may disturb the interaction between the CTS and AgnP, and no positive charges are being induced by CTS to the nanoparticles. Therefore, less damage to the cell membrane is produced by the individual components, making the antibacterial activity of this composite less effective. As shown by FTIR analysis, composites with filler content below 1 wt % do not show evidence of chemical interaction between the fillers and the matrix, and for CTS/CNT-AgnP composites, 1 wt % filler is the concentration with the best performance against bacteria. Above this concentration, both the formation of agglomerate and the interaction between CNT and AgnP reduce the antibacterial effectiveness.

As the CTS/CNT-AgnP 1 wt % composite showed the best antibacterial activity, the inhibition activities of these composites and commercial antibiotics against *S. aureus* are compared in Figure 12. The concentration of each antibiotic is given in the graph. The results show that the synthesized composite evaluated at 5 µg possesses higher inhibition activity than *ampicillin*, *cephalothin*, *cefotaxime*, *tetracycline*, *vancomycin*, *sulfamethoxazole* and *trimethoprim,* which were all evaluated at concentrations above 5 µg. Similarly, the activity against *E. coli* was compared with commercial antibiotics (not shown), and better results were obtained for the composite compared with the antibiotics.

The antibacterial activity of the composites presented here is comparable and in some cases superior to some polymer matrix composite materials recently reported. Anisha et al.[44] showed the antibacterial activity for a sponge composed of CTS, hyaluronic acid (HA) and nanosilver (nAg). They obtained the best performance against *E. coli* with a maximum inhibition diameter of 13 mm (CTS–HA/0.01% nAg composite), the same as our CTS/CNT-AgnP 0.5 wt % composite and lower than the CTS/CNT 0.5 wt % composite presented here [see Figure 11(a)]. Against *S. aureus*, the maximum inhibition diameter obtained in the CTS–HA-nAg composite was 14 mm,[44] which is slightly higher than the CTS/CNT 0.5 wt % composite, equal to the CTS/CNT-AgnP 0.5 wt % composite [Figure 11(b)] but lower than the CTS/CNT-AgnP 1 wt % composite presented in Figure 11(b). Das et al.[45] used the diffusion disc method to investigate the effect of CTS/silver nanocomposites against *P. aeruginosa*, *S. enterica* and *S aureus*. They found that the porous nanocomposite films exhibited superior antibacterial properties against Gram-negative bacteria compared with Gram-positive bacteria, but the inhibition diameters observed in the photographs are very small and no numerical value is given.

Erdohan et al.[46] used olive leaf extract (OLE) as an antimicrobial agent in polylactic acid (PLA) films and against *S. aureus*. They concluded that increasing the amount of OLE in the film

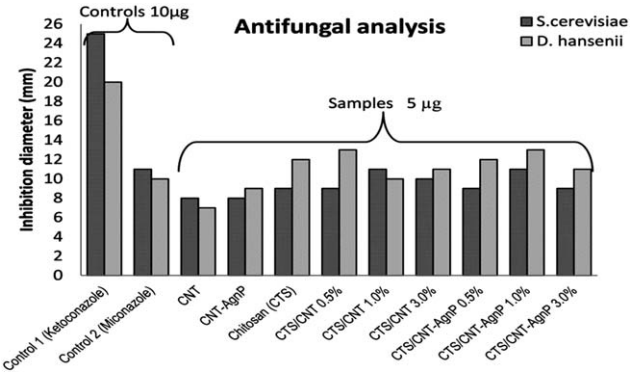

Figure 13. Antifungal analyses for CTS, CNT, CTS/CNT, CTS/CNT-AgnP composites, and controls.

discs from 0.9 to 5.4 mg produced a significant increase in the inhibitory zones from 9.10 to 16.20 mm, respectively. This inhibition diameter is comparable to the inhibition diameter of CTS/CNT-AgnP 1 wt % composite (5 µg) with the best performance in this study. Lately, the antimicrobial activity of polyaniline (PANI)-based conducting polymers has also been recorded.[47,48] However, Gizdavic-Nikoladis et al.[17] demonstrated better antimicrobial and antioxidant properties for functionalized PANIs (fPANIs). Meanwhile, Tamboli et al.[49] evaluated the antibacterial activity of a Ag–PANI nanocomposite against *B. subtilis*. The inhibition zone was between 10 and 18 mm in diameter around the disc with 25 µg and greater than that of Ag-PANI. Our triad CTS/CNT-AgnP 1 wt % (5 µg) was also tested against this bacillus, obtaining an inhibition diameter of 15 mm (not shown).

The mechanism of action of these CTS-based composites against bacteria is not well understood, and a synergistic effect of the three components would be expected; however, it seems that the chemical interaction between the silver nanoparticles and CNTs hinders this activity.

The inhibition diameters for the antifungal analysis of pristine CTS, CNT, CNT-AgnP and CTS/CNT and CTS/CNT-AgnP composites as well as the comparison with commercial controls are shown in Figure 13. The concentration of controls used was 10 µg, compared with 5 µg of our samples. Slightly better results against *D. hansenii* can be observed, and better results were obtained against this yeast with CTS/CNT 0.5 wt % and CTS/CNT-AgnP 1 wt % composites compared with the activity of the individual components. In these cases, the inhibition diameter changes from 7 mm for pristine CNT to 13 mm for CTS/CNT 0.5 wt %, from 9 for CNT-AgnP to 13 mm for CTS/CNT-AgnP 1 wt % and from 12 mm for pristine CTS to 13 mm for CTS composites. Compared with the controls, in all cases, the inhibition was better than miconazole, taking into account that the weight of the controls used was higher.

For *S. cerevisiae,* the composites CTS/CNT 1 wt % and CTS/CNT-AgnP 1 wt % were more active compared with pristine CTS, pristine CNT and CNT-AgnP. In this case, the diameter changed from 7 mm for pristine CNT to 11 mm for the CTS/CNT composite, from 7 mm for CNT-AgnPs to 11 mm for the CTS/CNT-AgnP composite and from 9 mm for pristine CTS to 11 mm for both composites. Compared with the weight of miconazole used, in all cases, better activity against this yeast was observed. However, for both yeasts, ketoconazole inhibition was superior. These inhibition diameters are competitive with the inhibition diameters reported for MCNTs functionalized with lysine and arginine.[50]

Galván-Márquez et al.[51] proposed a mechanism of action of CTS against *S. cerevisiae*. They stated that it is due to the disruption of protein synthesis by CTS in the cell membrane, with a minimum inhibitory concentration of 1.5 mg/mL. Sanone et al.[52] determined that the activity of CTS against fungi is due to the electrostatic interaction of the protonated amino groups of CTS with the negatively charged cell wall surface of the targeted microorganisms, which can lead to the disruption of the cell wall and therefore to cell death. Thus, in the literature, it has been concluded that the polycationic feature of CTS and CTS derivatives is fundamental for its antifungal activity,[53] and the effectiveness of CTS is real but complicated to control, as it depends not only on the CTS formulation but also on the fungus type and on the type of treatments (coating or film).[52,53] On the other hand, CNT have been successfully used in composites with a ceramic matrix as filters.[54] The performance of these new filters was assessed for the removal of yeast and heavy metals from water, and the results demonstrated that CNT plays the decisive role in the filter. It was also found that yeast cells were physically captured and immobilized by the tangled CNT networks. The mechanism of antifungal activity may be due to the disruption of the intracellular metabolic pathway, with oxidative stress as well as physical membrane damage causing rupture,[55] whereas Kim et al.[56] suggest that silver nanoparticles exert an antifungal activity by disrupting the structure of the cell membrane and inhibiting the normal budding process due to the destruction of the membrane's integrity.

In our composites formed by CTS, CNT, and AgnP, a synergistic effect of the three components was expected, but such a synergy is not fully demonstrated by the results. This result could be ascribed to the strong chemical interaction between Ag and CNT that limits the antifungal activity of the composites.

CONCLUSIONS

The dielectric properties of CTS-based composites have been analyzed from 20 to 250°C in the 0.1 to 10^6 Hz frequency range. CNTs decorated with silver nanoparticles by the microwave method were incorporated into pristine CTS at different concentrations to obtain bionanocomposite films. FTIR analysis revealed a strong interaction between CNT and AgnP, which in turn directly affects the conductivity enhancement of CTS/CNT-AgnP composites compared with CTS/CNT films, contrary to expectations. This chemical interaction between CNT and AgnP also affects the antibacterial activity of the composites. The α- and σ-relaxation are disclosed in CTS/CNT and CTS/CNT-AgnP composite film processes, in agreement with pristine CTS behavior. These relaxation processes are affected in the vicinity of the percolation threshold but not observed for composites with concentrations greater than 2 wt %. The Vogel temperature was observed to be more strongly influenced by the wt % of the

filler (either CNT or CNT-AgnP) compared with the water content. This temperature increases as the wt % increases as a result of the restricted motion of the main polymer chains due to their chemical interaction with the fillers. Finally, the antibacterial activity of CTS/CNT-AgnP composites, especially at 1 wt % filler, seems to be competitive with respect to commercial antibiotics, and their antifungal activity is considerable. This evidence supports the effectiveness of these composites in potential applications where hygiene is important.

ACKNOWLEDGMENTS

The authors thank J. A. Muñoz-Salas, R. A. Mauricio Sánchez, and M. del C. Delgado-Cruz for their technical assistance with the electrical, FTIR, and TGA measurements, respectively. This work was supported by Consejo Nacional de Ciencia y Tecnología of México (CONACYT), Grant #150767.

REFERENCES

1. Erdema, A.; Mutia, M.; Karadeniza H.; Congura, G.; Canavara, E. *Colloid. Surf. B Biointer.* **2012**, *95*, 222.
2. Pauliukaite, R.; Ghica, M. E.; Fatibello-Filho, O.; Brett, C. M. A. *Electrochim. Acta* **2010**, *55*, 6239.
3. Carson, L.; Kelly-Brown, C.; Stewart, M.; Oki, A.; Regisford, G.; Luo, Z.; Bakhmutov, V. I. *Mat. Lett.* **2009**, *63*, 617.
4. Wang, S. F.; Shen, L.; Zhang, W. D.; Tong, Y. *J. Biomacromolecules* **2005**, *6*, 3067.
5. Shieh, Y. T.; Yang, Y. F. *Eur. Polym. J.* **2006**, *42*, 3162.
6. Hao, C.; Ding, L.; Zhang, X.; Ju, H. *Anal. Chem.* **2007**, *79*, 4442.
7. Ke, G.; Guan, W.; Tang, C.; Guan, W.; Zeng, D.; Deng, F. *Biomacromolecules* **2007**, *8*, 322.
8. Liu, Y. L.; Chen, W. H.; Chang, Y. H. *Carbohydr. Polym.* **2009**, *76*, 232.
9. Tang, C.; Chen, N.; Zhang, Q.; Wang, K.; Fu, Q.; Zhang, X. *Polym. Degr. Stab.* **2009**, *94*, 124.
10. Perez, C.; Prokhorov, E.; Luna-Bárcenas, G.; González-Campos, J. B.; Sanchez, I.C.; Gonzalez-Hernandez, J.; Mendoza Duarte, M. E.; Villaseñor-Ortega, F. *J. Nanostr. Polym. Nanocomp.* **2010**, *6*, 61.
11. Zhang, W.; Li, W.; Wang, J.; Qin, C.; Dai, L. *Fibers Polym.* **2010**, *11*, 1132.
12. Chen, L.; Yu, W.; Xie, H. *Powd. Tech.* **2012**, *231*, 18.
13. Kim, K. S.; Park, S.; Jin, J. *Solid State Chem.* **2011**, *184*, 2724.
14. Lin, J.; He, C.; Zhao, Y.; Zhang, S. *Sens. Act. B* **2009**, *137*, 768.
15. Basavaraja, C.; Jo, E. A.; Kim, B. S.; Kim, D. G.; Huh, D. S. *Macromol. Res.* **2010**, *18*, 222.
16. Campoccia, D.; Montanaro, L.; Arciola, C. R. *Biomaterials* **2013**, *34*, 8533.
17. Gizdavic-Nikolaidis, M. R.; Bennet, J. R.; Swift, S.; Easteal, A. J.; Ambrose, M. *Acta Biomater.* **2011**, *7*, 4204.
18. Gizdavic-Nikolaidis, M. R.; Bennett, J.; Zujovic, Z.; Swift, S.; Bowmaker, G. A. *Synth. Met.* **2012**, *162*, 1114.
19. González-Campos, J. B., Mota-Morales, J. D., Kumar, S.; Zárate-Triviño, D.; Hernández-Iturriaga, M.; Prokhorov, E.; Vazquez-Lepe, M.; García-Carvajal, Z. Y.; Sanchez, I. C.; Luna-Bárcenas, G. *Colloid Surf. B Biointer.* **2013**, *111*, 741.
20. Pal, S.; Kyung, Y.; Song, J. M. *J. Appl. Environ. Microbiol.* **2007**, *73*, 1712.
21. Lagaron, J. M.; Fernández-Saiz, P.; Ocio, M. J. *J. Agric. Food Chem.* **2007**, *55*, 2254.
22. Leceta, I.; Guerrero, P.; Ibarburu, I.; Dueñas, M. T.; de la Caba, K. *J. Food Eng.* **2013**, *116*, 889.
23. González-Campos, J. B., Prokhorov, E.; Luna-Bárcenas, G.; Sanchez, I. C.; Lara-Romero, J.; Mendoza-Duarte, M. E.; Villaseñor, F.; Guevara-Olvera, L. *J. Appl. Polym. Sci. Part B: Polym. Phys.* **2011**, *48*, 739.
24. Shieh, Y. T.; Wu, H. M.; Twu, Y. K.; Chung, Y. C. *Colloid Polym. Sci.* **2010**, *288*, 377.
25. Efros, A. L.; Shklovskii, B. I. *Phys. Status Solid B* **1976**, *76*, 475.
26. González-Campos, J. B.; Prokhorov, E.; Luna-Bárcenas, G.; Mendoza-Galván, A.; Sanchez, I. C.; Nuño-Donlucas, S. M.; García-Gaitan, B.; Kovalenko, Y. *J. Polym. Sci. Part B: Polym. Phys.* **2009**, *47*, 932.
27. González-Campos, J. B.; Prokhorov, E.; Luna-Bárcenas, G.; Fonseca-García, A.; Sanchez, I. C. *J. Polym. Sci. Part B: Polym. Phys.* **2009**, *47*, 2259.
28. Lau, C.; Cooney, M. J.; Atanassov, P. *Langmuir* **2008**, *24*, 7004.
29. Piri, N.; Mottaghitalab, V.; Arbab, S. *Fibers Polym.* **2013**, *14*, 236.
30. Potara, M.; Jakab, E.; Damert, A.; Popescu, O.; Canpean, V.; Astilean, S. *Nanotechnology* **2011**, *22*, 135101.
31. Kirkpatrick, S. *Rev. Mod. Phys.* **1973**, *45*, 574.
32. Stauffer, D.; Aharony, A. Introduction to Percolation Theory; Taylor & Francis: London, **1994**.
33. Gonon, P.; Boudefel, A. *J. Appl. Phys.* **2006**, *99*, 024308.
34. Kim, Y. J. Shin, T. S.; Choi, H. D.; Kwon, J. H.; Chung, Y. C.; Yoon, H. G. *Carbon* **2005**, *43*, 23.
35. Prokhorov, E.; Luna-Bárcenas, J. G.; González-Campos, J. B.; Sanchez, I. C. *Mol. Cryst. Liq. Cryst.* **2011**, *536*, 24.
36. Einfeldt, J.; Meiner, D.; Kwasniewski, A. *Prog. Polym. Sci.* **2001**, *26*, 1419.
37. Raju, G. G. Dielectrics in Electrical Fields; Marcel Dekker, Inc.: New York, **2003**; p 260.
38. Padmasree, K. P.; Kanchan, D. K. *Mat. Sci. Eng. B* **2005**, *122*, 24.
39. Köhler, M.; Lunkenheimer, P.; Loidl, A. *Eur. Phys. J. E* **2008**, *27*, 115.
40. Wei, D.; Sun, W.; Qian, W.; Ye, Y.; Ma, X. *Cabohydr. Res.* **2009**, *344*, 2375.
41. Kang, S.; Herzberg, M.; Rodrigues, D. F.; Elimelech, M. *Langmuir* **2008**, *24*, 6409.
42. Zhu, X.; Bai, R.; Wee, K. H.; Liu, C.; Tang, S. L. *J. Membr. Sci.* **2010**, *363*, 278.

43. Morones, J. R.; Elechiguerra, J. L.; Camacho, A.; Holt, K.; Kouri, J. B.; Tapia, R. J.; Yacaman, J. M. *Nanotechnology* **2005**, *16*, 2346.
44. Anisha, B. S.; Biswas, R.; Chennazhi, K. P.; Jayakumar, R. *Int. J. Biol. Macromol.* **2013**, *62*, 310.
45. Das, S.; Das, M. P.; Das, J. *Pharm. Res.* **2013**, *6*, 11.
46. Erdohan, Z. Ö.; Cam, B.; Turhan, K. N. *J. Food Eng.* **2013**, *19*, 308.
47. Gizdavic-Nikolaidis, M.; Travas-Sejdic, J.; Bowmaker, G. A.; Cooney, R. P.; Kilmartin, P. A. *Synth. Metals* **2004**, *140*, 225.
48. Gizdavic-Nikolaidis, M.; Travas-Sejdic, J.; Bowmaker, G. A.; Cooney, R. P.; Thompson, C.; Kilmartin, P. A. *Curr. Appl. Phys.* **2004**, *4*, 347.
49. Tamboli, M. S.; Kulkarni, M. V.; Patil, R. H.; Gade, W. N.; Navale, S. C.; Kale, B. B. *Colloid Surf. B: Biointer.* **2012**, *92*, 35.
50. Zare-Zardini, H.; Amiri, A.; Shanbedi, M.; Memarpoor-Yazdi, M.; Asoodeh, A. *Surf. Inter. Anal.* **2013**, *45*, 751.
51. Gálvan-Márquez, I.; Akuaku, J.; Cruz, I.; Cheetham, J.; Golshani, A.; Smith, M. L. *Int. J. Food Microbiol.* **2013**, *164*, 108.
52. Sansone, F.; Picerno, P.; Mencherini, T.; Porta, A.; Lauro, M. R.; Russo, P.; Aquino, R. P. *J. Food Eng. 2014*, 120, 260.
53. Tayela, A. A.; Moussa, S.; El-Tras, W. F.; Knittel, D.; Opwis, K.; Schollmeyer, E. *Int. J. Biol. Macromol.* **2010**, *47*, 454.
54. Parham, H.; Bates, S.; Xia, Y.; Zhu, Y. *Carbon* **2013**, *54*, 215.
55. Zare-Zardini, H.; Amiri, A.; Shanbedi, M.; Memarpoor-Yazdi, M.; Asoodeh, A. *Surf. Interface Anal.* **2013**, *45*, 751.
56. Kim, K. J.; Sung, W. S.; Suh, B. K.; Cee, D.G. *Biometals* **2009**, *22*, 235.